Exploiting Acetal Moieties for the Synthesis of Degradable-On-Demand Polymeric Architectures

Angela Romano,[a] Stefano Frattini,[a] Roberto Miani,[b] Claudio Gioia,*[b] Annamaria Celli,[a] and Laura Sisti[a]

Developing polymers with labile bonds has attracted increasing attention since it can favor the chemical recycling into oligomers or even the starting monomers that could be recovered and re-used. Different chemical bonds can break upon exposure to external stimuli, such as thermal, UV, or chemical triggers. Among these, the acetal bond can degrade under mild acidic conditions. This study focuses on the synthesis of polymers constituted by acetal moieties suitable for triggered depolymerization. In particular, the solvent-less poly-addition of 1,4-butanediol and 1,4-butanediol divinyl ether was developed and optimized using a heterogeneous catalyst (Amberlyst 15) at 100 °C. The best reaction conditions in terms of catalyst loading and reagent ratio were determined through a Design-of-Experiment aiming to achieve high conversion, low polydispersity, and desirable molecular weight. The resulting material presented an amorphous character and thermal stability up to 220 °C. It was confirmed responsive in an acidic environment, being completely hydrolyzed in 42 days, while remaining stable at neutral and basic pH. The obtained results represent a proof of concept for the design of pH-responsive materials through solventless, and scalable processes. The acetal moiety may be further exploited to achieve architectures presenting a sustainable end-of-life by implementing a recycling-by-design approach for new adhesives or novel degradable thermosetting materials.

Introduction

Crosslinked materials are widely used in composites, electronic packaging, coatings, adhesives, and rubbers, accounting for 18% of the total worldwide polymer production. Thanks to their structure, they present excellent thermal, and mechanical properties along with enhanced chemical resistance.[1] While their strategic exploitation is crucial for the development of a variety of materials, the sustainability of their end-of-life is currently raising concerns. Indeed, since post-consumer thermosets are impossible to melt-process and recycle, most of them end up being incinerated or disposed of in landfills,[2] along with all the materials designed to be permanently coupled with them. The accumulation of thermoset plastics in the environment poses a significant threat that must be addressed by transitioning towards a sustainable circular economy. This transition requires the development of new strategies for the re-use and recycling of such materials at the end of their life.[3] In this context, a strategy can be based on the closed-loop recycling to monomers that can ensure the recovery of polymer building blocks.[4] In the case of thermoplastic polyesters or polyamides, for example, the hydrolysis or glycolysis reactions have been developed to break the ester and amide bonds.[6] This approach can be applied to thermoset materials by integrating cleavable bonds that can break under specific conditions to de-crosslink the molecular network. Indeed, novel approaches have focused on developing materials with de-bonding properties by exploiting thermal, UV, or chemical external stimuli.[2,8]

When it comes to adhesives, debond-on-demand materials have garnered significant interest, due to their numerous economic and environmental advantages. Several approaches have been reported to obtain this property, e.g. pressure-sensitive adhesives, photodegradable adhesives, biodegradable adhesives, and adhesives containing reversible covalent bonds.[10] Kaiser and Ginzinger recently developed an adhesive consisting of maleimide- and furan-functionalized polyurethane pre-polymers that cure through the Diels–Alder reaction to be used in a multi-layer packaging material. This material could then be delaminated by partially opening the Diels–Alder adducts through the influence of temperature.[12] Other degradable-on-demand materials have been prepared using the Diels-Alder chemistry,[13] transesterification,[15] imine bonds[17] or acetal linkages.[19]

The acetal bond, which is the object of this study, can be formed via acidic catalysis through different reactions addition,[21] condensations,[23] and transacetalization.[24] The most commonly used catalysts are Brønsted acids, i.e. H_2SO_4, HCl, H_3PO_4, and p-toluenesulfonic acid,[25] however also Lewis acids, transition metal complexes, and redox catalytic systems can be exploited.[26] The use of an acidic catalyst requires a

[a] Department of Civil, Chemical, Environmental and Materials Engineering, University of Bologna, Bologna, Italy

[b] Department of Physics, University of Trento, Povo, TN, Italy

Correspondence: Dr. Claudio Gioia, Department of Physics, University of Trento, Via Sommarive 14, 38123 Povo, TN, Italy.
Email: claudio.gioia@unitn.it

work-up at the end of the reaction to separate it from the product, as acids in the presence of water can degrade the acetal bond. Indeed, the nucleophilic attack of water on the acetal bond causes the formation of an alcohol and a hemi-acetal, which is unstable and further reacts to aldehyde and alcohol.[27] The presence of acetal bonds in polymers dates back to 1912 when Read reported about a product of very high molecular weight obtained from the condensation of glyoxal and pentaerythritol.[28] Since then, polyacetals have been prepared via different synthetic approaches, both as thermo-plastic materials and as crosslinked structures. These materials employ the labile nature of the bond in acidic conditions for applications in the biomedical field, lithography,[29] as drug delivery carriers,[30] in the preparation of elastomeric materials,[31] and more recently in the development of recover-able adhesives.[33]

This promising class of materials can be obtained through different strategies. The polycondensation reaction between a diol and a carbonyl compound is widely used but requires a distillation step to remove the water formed as a side product. Similarly, transacetalization between a diol and an acetal compound also generates alcohols as side products.[34] Poly-acetals can also be prepared via cationic ring-opening polymer-ization starting from a cyclic acetal,[35] however, this synthesis can lead to side reactions and the formation of different cyclic compounds. Other methods are the polyaddition of a diol and a divinyl ether, or the step-growth polymerization of a hydroxy vinyl ether,[37–38] which avoids the formation of side products. Moreover, divinyl ether can react with dicarboxylic acids to obtain poly(hemiacetal esters).[39] Ruckenstein and Zhang, for example, studied the "click" polyaddition of ethylene glycol, divinyl ether, and a diphenol or a diol in THF, in the presence of pyridinium p-toluenesulfonate as a catalyst.[37] A self-poly addition of vinyl ethers with a hydroxyl group in THF with p-toluene sulfonic anhydride led to the formation of a high molecular weight polyacetal.[38] A series of linear water-soluble polyacetals were synthesized in anhydrous dichloromethane using pyridinium p-toluenesulfonate as the catalyst.[30] More recently, a polymer with acetal functions was prepared using diphenyl phosphate as an acidic catalyst.[40] In all cases, the use of homogeneous catalysts required a multi-step work-up for the neutralization and separation of the catalyst, which could have caused degradation of the polymer. Moreover, the use of solvents, such as THF or dichloromethane, makes the process not sustainable and difficult to scale up. Indeed, a solvent-less reaction coupled with an easy separation of the catalyst could allow the development of a simpler and more sustainable process with promising applications.

Framed in this background, this study focuses on the synthesis of polymers with acetal moieties suitable for a triggered depolymerization, that could be applied in the future as main constituents of debond-on-demand adhesives or recyclable thermosetting materials. The strategy is based on developing a green synthesis for preparing polymers containing acetal bonds via bulk polymerization without using solvents. In particular, starting from a diol and a divinyl ether with the same aliphatic chain length (1,4-butanediol and 1,4-butanediol divinyl

ether), the solvent-less polyaddition was initially optimized in terms of catalyst, reagents molar ratio, and temperature. Furthermore, a Design of Experiment (DoE) was used to optimize the amount of catalyst and the reagents molar ratio to maximize the conversion, minimize the polydispersity, and achieve the desired molecular weight of the material. The thermal properties of the polyacetal obtained in the best reaction conditions were then evaluated via thermal gravimetric analysis (TGA) and differential scanning calorimetry (DSC), as well as the hydrolytic degradability after incubation at pH 4, 7, and 10.

Experimental Section

Materials

1-butanol, n-butyl vinyl ether, 1,4-butanediol (BD), 1,4-butane-diol divinyl ether, H_3PO_4 (85% w/w), titanium butoxide (TBT), H_2SO_4 (98%), $CHCl_3$, ethyl acetate (EtOAc), anhydrous $NaSO_4$, NaCl and Amberlyst 15 (Amb-15) (4.7 meq g^{-1}) were purchased from Sigma-Aldrich and were used without further purification.

Synthesis of 1-(1-butoxyethoxy)Butane (MC-1)

Before the reaction, glassware and Amberlyst 15 were dried in the oven overnight. 1-butanol (2 g, 27.0 mmol, 1 eq), n-butyl vinyl ether (2.97 g, 29.7 mmol, 1.1 eq), and Amberlyst 15 (Amb-15) (29 mg, 0.5 mol%) were put in a round-bottom flask. Next, the reaction mixture was put under N_2 flow for 5 minutes under magnetic stirring, and then in an oil bath at 75°C. The reaction was monitored via FT-IR to check the disappearance of the signal related to the C-C stretching (1620–1640 cm^{-1}). At the end of the reaction, the catalyst was separated from the product via centrifuge (10000 rpm, 2 min). The sample (Model Compound-1, MC-1) was analyzed via ^{1}H-NMR spectroscopy.

^{1}H-NMR (400 MHz, CDCl$_3$, δ): 0.95 (t, 3H, CH$_3$), 1.30 (d, 3H, CH$_3$), 1.38 (m, 2H, CH$_2$), 1.57 (m, 2H, CH$_2$), 3.41–3.58 (m, 2H, CH$_2$), 4.67 (dd, H, CH).

Synthesis of Polyacetal (PAc)

Before the reaction, the glassware was dried in the oven overnight. 1,4-butanediol and 1,4-butanediol divinyl ether were put in a round-bottom flask. Next, the reaction mixture was put under N_2 flow for 5 minutes under magnetic stirring, and then in an oil bath. The catalyst was added. The reaction was monitored via FT-IR to check the disappearance of the signal related to the C-C stretching (1620–1640 cm^{-1}). The products were analyzed via ^{1}H-NMR spectroscopy. Three different param-eters were screened:

– Type of catalyst: Amberlyst 15 (12 mg), H_3PO_4, H_2SO_4, and TBT (two drops). In the case of Amberlyst 15, at the end of the reaction, the catalyst was separated from the product via centrifuge (10000 rpm, 2 min);

ChemSusChem

Research Article
doi.org/10.1002/cssc.202402154

Chemistry
Europe
European Chemical
Societies Publishing

– BD/divinyl ether molar ratios (Table 1
–);
– Temperature kinetics tests were performed by measuring the M_w via GPC at 50 and 100 °C.

The polyacetal (PAc) was prepared in the best conditions. 1,4-butanediol (1 g, 11.1 mmol, 1 eq), 1,4-butanediol divinyl ether (1.73 g, 12.2 mmol, 1.1 eq), and Amberlyst 15 (0.5 mol%) were introduced in a round-bottom flask. Next, the reaction mixture was put under N_2 flow for 5 minutes under magnetic stirring, and then in an oil bath at 100 °C. At the end of the reaction (45 min), the crude product was dissolved in 50 mL of EtOAc and the catalyst was filtered. The solvent was evaporated under reduced pressure. Finally, the cyclic acetal side product was separated at 50 °C under vacuum. The product was analyzed via ^{1}H-NMR and GPC. ^{1}H-NMR (400 MHz, CDCl$_3$, δ): 1.28 (d, 3H, CH$_3$), 1.62 (m, 2H, CH$_2$), 3.41–3.58 (m, 2H, CH$_2$), 4.67 (dd, H, CH).

Degradation Study

Polyacetal (200 mg) (PAc) was introduced in a vial containing 2 mL of aqueous buffer solutions at different pH, namely 4, 7, and 10, forming a heterogeneous mixture maintained under vigorous stirring. After 24 h, a polymer sample was collected by a spatula, dissolved in CHCl$_3$, and dried with anhydrous NaSO$_4$. The molecular weight was measured via GPC. The Mw (%) was calculated as the ratio between the molecular weight Mw at a specific sampling time and the initial one.

Characterization

Number average molecular weight (M$_n$), weight average molecular weight (M$_w$), and polydispersity index (PD) were measured by gel permeation chromatography (GPC) performed in CHCl$_3$ at ambient temperature, using a Knauer Azura apparatus with a PL gel 5 μm Minimixed-C column and a refractive index detector. Polystyrene standards were employed for preparing a universal calibration curve. The lower limit of the operating range of the column was 500 g mol^{-1}. The ^{1}H NMR spectra were acquired using a Varian Mercury 400 spectrometer, and the chemical shifts were reported in ppm downfield from tetramethylsilane (TMS); the solvent used was CDCl$_3$. FT-IR analysis was performed over the wavenumber range of 650–4000 cm^{-1} using a Perkin Elmer Spectrum One

spectrometer equipped with a Universal ATR Sampling Accessory. Each spectrum was obtained from 8 scans. The calorimetric analysis (DSC) was carried out using a Perkin-Elmer DSC7. Measurements were conducted under nitrogen flow. The sample (around 10 mg) was kept at −100 °C for 2 min, then heated up to 100 °C (at 20 °C min^{-1}), kept at high temperature for 1 min, and then cooled down to −100 °C (at 10 °C min^{-1}). Then, the 2nd scan was carried out and the sample was heated up to 100 °C (at 10 °C min^{-1}). The glass transition temperature (T$_g$) was measured during the 2nd heating scan and was taken as the midpoint of the heat capacity increment associated with the glass-to-rubber transition.

Thermogravimetric analysis (TGA) was carried out under nitrogen flow (40 mL min^{-1}) using a Perkin Elmer TGA4000 apparatus, in the range of 50–900 °C with a heating rate of 10 °C min^{-1}. The onset degradation temperature (T$_{onset}$) was measured from the intersections of the tangents of the initial points and the inflection points.
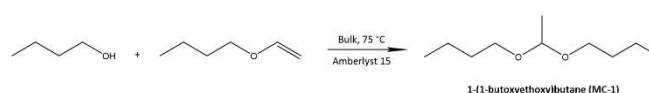
Optimization via DoE

The design of Experiment (DoE) was performed using Minitab 21 software. Experimental data were analyzed estimating a 95% confidence interval. T-test was used to determine the significance of the regression coefficients and the associated probabilities (p-values). The model equation significance was determined by Fisher's test (F test). The variance explained by the model is given by the multiple determination coefficients, R^2. For each test, the sample was analyzed in triplicate via GPC, and the molecular weight M$_w$ was calculated as the mean value.

Results and Discussion

Synthesis of the Polyacetal Architecture

The addition of 1-butanol to n-butyl vinyl ether (Scheme 1) was selected as the model reaction to represent the target polymerization. In particular, the conversion of the vinyl ether was studied in bulk, at 75 °C, in the presence of Amberlyst 15 (Amb-15) as an acid catalyst. This setup was used to evaluate the yield of the desired acetal adduct and thus understand the feasibility of the reaction.

The reaction was monitored via FT-IR, by observing the disappearance of the signal related to C-C stretching (1610–1620 cm^{-1}).[41] The formation of acetal bond was observed via the signal related to C-O-C stretching at 1050–1150 cm^{-1} (Figure 1A).[42] The formation of 1-(1-butoxyethoxy)butane (MC-1) was also confirmed by ^{1}H-NMR analysis (Figure 1B). More in detail, the signal at 4.67 ppm is related to the H$_a$ of the methine

Table 1. Screening of reagents molar ratio.		
Test	1,4-butanediol (eq)	1,4-butanediol divinyl ether (eq)
1	1.00	1.20
2	1.00	1.10
3	1.00	1.05
4	1.00	1.00
5	1.10	1.00

Scheme 1. Synthesis of MC-1.

ChemSusChem

Research Article
doi.org/10.1002/cssc.202402154
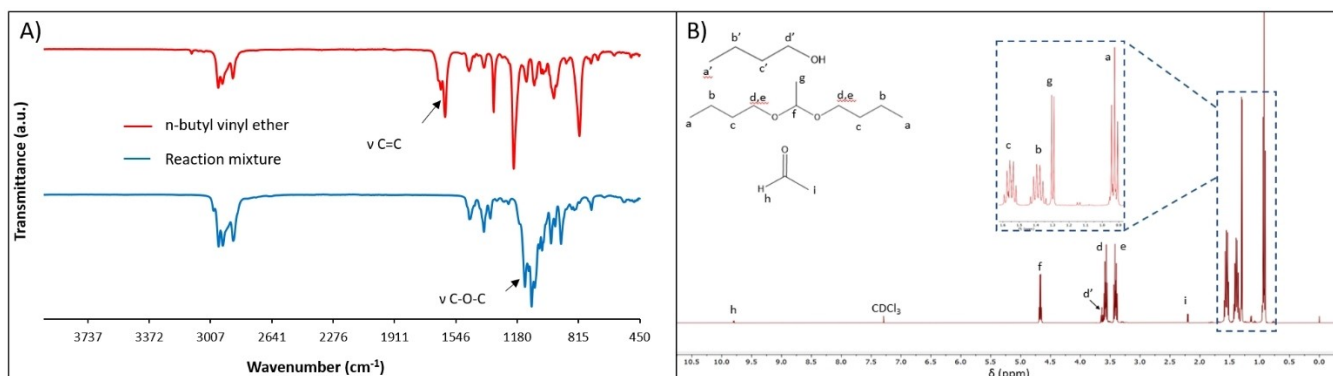
Chemistry
Europe
European Chemical
Societies Publishing

Figure 1. A) FT-IR spectra of n-butyl vinyl ether and the model reaction mixture; B) ^{1}H-NMR spectrum of the model reaction mixture.

and the signal at 1.30 ppm to H_f of the methyl group of acetal moieties.[40] The CH$_2$ protons next to the acetal group are diastereotopic (H_c and $H_{c'}$), according to their proximity to the methyl or methine groups, thus they present two different signals at 3.58 and 3.41 ppm. The presence of acetaldehyde is
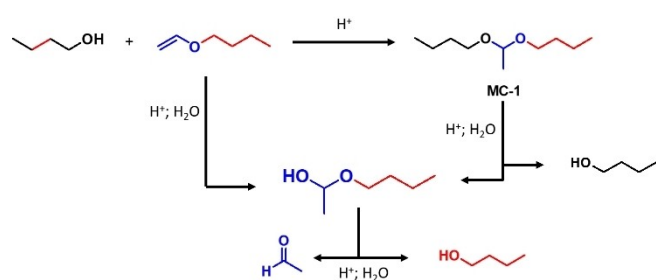
Scheme 2. Possible degradation pathways for n-butyl vinyl ether and MC-1.
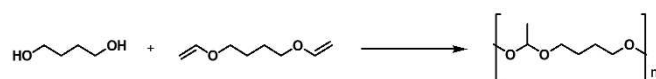
Scheme 3. Synthesis of polyacetal.

also detected at 2.20 and 9.80 ppm, which could result from the degradation of the acetal or the vinyl ether. In both cases, degradation occurs in acidic conditions and the presence of water, forming the unstable intermediate hemiacetal, which further degrades to alcohol and acetaldehyde (Scheme 2).[27,43]

The information achieved through the model reaction was then applied to develop a first attempt at the development of an acetal-based polymer deriving from the step-growth polyaddition of 1,4-butanediol (BDO) and 1,4-butanediol divinyl ether (BDVE) (Scheme 3).

Since the formation of acetal bonds in polymers is favored in acidic conditions,[30,37,44–49] Brønsted acids (H$_3$PO$_4$, H$_2$SO$_4$, Amberlyst 15), and titanium tetra butoxide (TBT) as Lewis acid were initially tested and compared with a reference reaction performed in absence of the catalyst. The initial polymerization attempt was carried out in bulk at 100 °C to favor mixing due to the viscous character of the components. The results (Table 2, Entries 1–5) showed that only Brønsted acid catalysts can promote the reaction while no reaction was observed in the presence of TBT. More in detail, the blank reaction (without catalyst) did not produce any product while sulfuric acid promoted a prompt degradation of the components. The presence of phosphoric acid produced low molecular weight

Entry	BDVE/BDO	Cat	T (°C)	Reaction Time (min)	PAc Yield (%)	Mw (g mol^{-1})	PD
1	1.1	None	100	45	0	–	–
2	1.1	H$_3$PO$_4$	100	45	93	5200	1.65
3	1.1	H$_2$SO$_4$	100	Degradation	–	–	–
4	1.1	TBT	100	45	0	–	–
5	1.1	Amb-15	100	45	99	46000	2.43
6	1.0	Amb-15	100	45	n.a.	650	1.33
7	0.9	Amb-15	100	45	n.a.	2580	1.70
8[c]	1.1	Amb-15	100	5	4	n.a.	n.a.
9[c]	1.1	–	100	10	7	n.a.	n.a.
10[c]	1.1	–	100	20	4	n.a.	n.a.

Table 2. Explorative tests for the step-growth polyaddition of 1,4-butanediol (BDO) and 1,4-butanediol divinyl ether (BDVE).

[a] Determined by ^{1}H NMR; [b] Determined by GPC; [c] Entries 9, and 10 are different sampling times from Entry 8 after removing the catalyst by filtration; n.a. = not available.

ChemSusChem

Research Article
doi.org/10.1002/cssc.202402154

Chemistry Europe
European Chemical
Societies Publishing

oligomers while tests presenting a higher catalyst loading produced an insoluble material. Such behavior may be associated with undesired crosslinking processes deriving from the cationic polymerization of the vinyl moiety.[50] Indeed, Amberlyst 15 gave the best result, and a polyacetal with a molecular weight of 38000 g mol^{-1} was obtained. As reported in Entries 6 and 7, the step-growth polyaddition demonstrated pronounced differences in molecular weight according to the ratio of the starting components. Such behavior was also observed by Samanta et al., who managed to modulate the molecular weight of the materials by slightly varying the reagents ratio.[30] In any case, a slight excess of BDVE may be valuable to counterbalance its volatility which would create unbalances in the polymerization stoichiometry.

The effectiveness of the heterogeneous catalyst separation was verified, to understand if acid traces could still be present in the product after filtration (Table 2, Entries 8–10). In a dedicated experiment, Amb-15 was removed after 5 minutes of reaction. Afterward, the mixture was further monitored at 5, 10, and 20 minutes via ^{1}H-NMR (Figure S1). After catalyst removal, most of the reagent was still present and a small percentage of the polymer formed. At 10 and 20 minutes (Figure S1, green and blue curves, respectively), no substantial changes were observed, indicating that no catalyst traces were still present in the reaction mixture and that filtration was an efficient separation method to remove the catalyst.

A further step in understanding the polymerization concerned the effect of temperature. Two temperatures were investigated, i.e. 100 and 50 °C, by monitoring the polyacetal molecular weight over time (Figure 2). In both tests, Amberlyst 15 was used as a catalyst with a DBVE/BDO ratio of 1.1.

Figure 2 shows that polyacetal synthesis proceeds faster at 100 °C, with the molecular weight reaching high values (35000 g mol^{-1}) within 30 minutes and a maximum value (> 45000 g mol^{-1}) at 45 minutes. In contrast, at 50 °C the reaction shows a delay in polymerization initiation of about 45 min. These results were confirmed by monitoring the conversion of DBVE by ^{1}H-NMR analysis (Figures S3 and S4). Indeed, at 100 °C the percentage of divinyl ether drops in the first 10 minutes and reaches a plateau after 30 minutes (Figure S2). On the other hand, the conversion of divinyl ether percentage at 50 °C is low at the beginning and becomes consistent after 60 minutes.
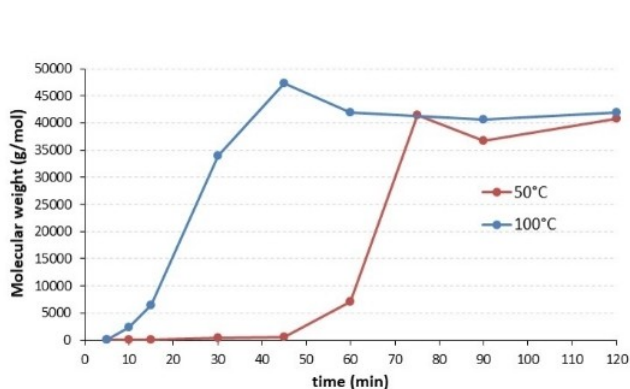
These results demonstrated that at 100 °C a consistent molecular weight can be obtained already after 30 min of polymerization.

The previously reported explorative tests were exploited to conceive a tentative procedure for producing the main polymeric product. However, an unexpected condensation product was detected on the flask ceiling. ^{1}H-NMR spectroscopy tests were performed to confirm the polymeric structure and to investigate any potential undesired reaction. Figure 3 shows the ^{1}H-NMR of the obtained material. The signal related to the methine group is visible at 4.67 ppm (H$_a$), together with the signal related to the methyl group at 1.30 ppm (H$_b$) of the acetal moieties. Moreover, as already observed for the molecular model, the CH$_2$ protons next to the oxygen are diastereotopic, thus they present two different signals at 3.41 (H$_c$) and 3.58 ppm (H$_{c'}$).

Figure 4 reports the ^{1}H-NMR study of the condensation product, recovered on the reactor ceiling. Indeed, the presence of the signals observed at 6.45, 4.17, and 3.96 ppm was associated with the unsaturated bonds of DBVE and confirmed its tendency to evaporate from the reaction mixture. Additional signals were ascribed to a cyclic acetal compound. In particular, the signal at 4.88 ppm could be related to the methine group (H$_f$) and the signal at 1.28 ppm to the methyl of the acetal group (H$_e$). This compound could form via two side reactions, both catalyzed by acids (Scheme 4): the intramolecular addition of the hydroxy vinyl ether, which forms from the degradation of the divinyl ether, and the intramolecular transacetalization.[51] Side reactions that lead to the formation of cyclic acetals and macrocycles via intramolecular addition have already been reported,[38,52] and these byproducts usually form in the first stage of the reactions, but the main intermolecular addition remains the main reaction that leads to a high molecular weight linear polyacetal.

The combination of the information achieved by the reported tests pictured a complex panorama of consecutive and parallel processes that may be involved during the step-growth polymerization of BDO and DBVE (Scheme 4, black), under the same acid catalysis. Indeed, DBVE can be subjected to several undesired processes able to consume and deplete it from polymerization. For example, the evaporation of DBVE
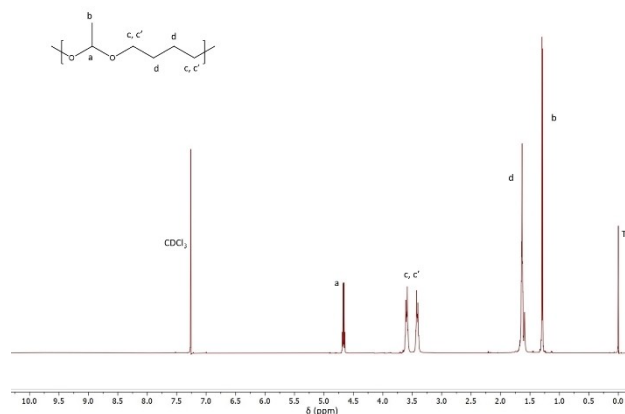
Figure 2. Evolution of polyacetal molecular weight at 100 and 50 °C monitored by GPC.

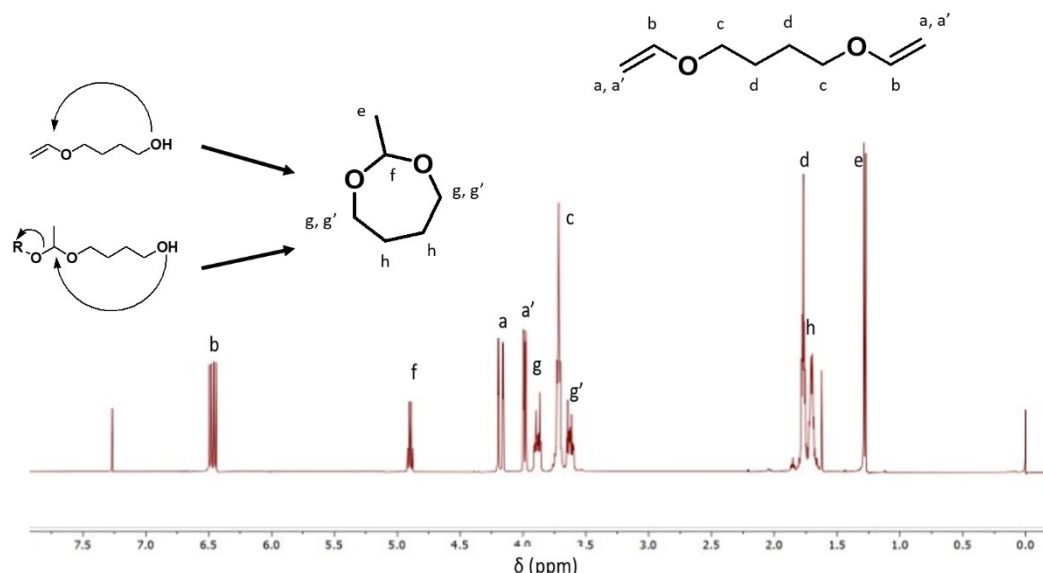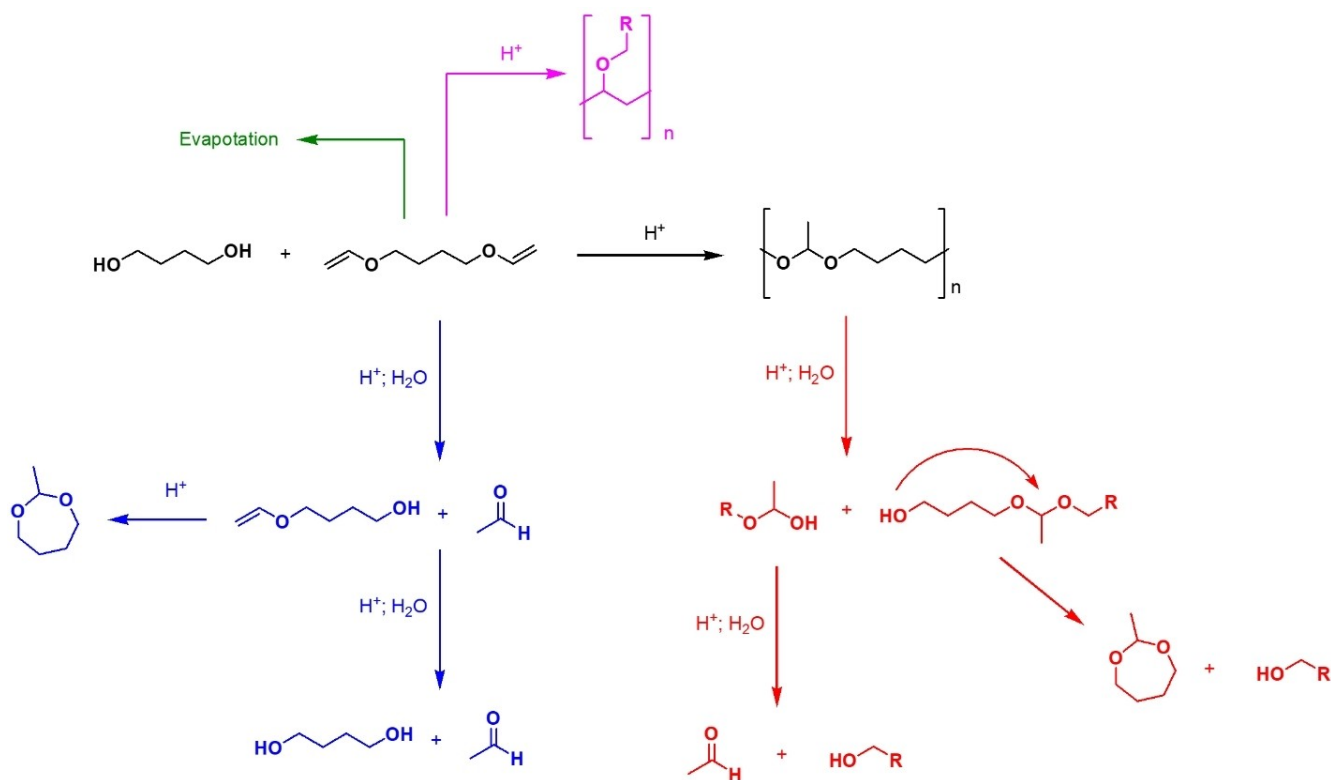**Figure 3.** ^{1}H-NMR spectrum of crude polyacetal prepared with Amberlyst 15.

Figure 4. ^{1}H-NMR spectrum of condensation products in the reactor ceiling during the polyacetal synthesis.

Scheme 4. Side reactions involved in the synthesis of polyacetal.

(Scheme 4, green) was observed as an undesired accumulation on the reactor ceiling while the degradation of the vinyl ether, acid-catalyzed in the presence of moisture traces, is responsible for the formation of alcohols, acetaldehyde, and the cyclic adduct (Scheme 4, blue). Furthermore, an excessive acid content could promote cationic oligomerization (Scheme 4, pink), creating *in situ* branched structures able to promote large polydispersity or even insoluble crosslinked materials. More-over, the acetal moiety of the desired polymer can be subjected to acid-catalyzed degradation processes (Scheme 4, red). In particular, in the presence of humidity in the reaction environment, the acetal is firstly degraded into hemiacetal, which is quickly decomposed in alcohols and aldehyde moieties.[27] Furthermore, the creation of alcoholic end-groups on the polymer structure can evolve into the formation of cyclic acetal compounds by intramolecular transacetalization.

ChemSusChem

Research Article
doi.org/10.1002/cssc.202402154

Chemistry Europe
European Chemical
Societies Publishing

Given the complexity of the depicted reactive pathways, the acid catalyst loading, being involved in all the undesired processes, as well as the reagent ratio emerge as the most critical parameters affecting the polymerization success. A further dedicated optimization by Design of Experiment (DOE) was performed to specifically understand the influence of these key variables on conversion, molecular weight, and polydispersity.

Process Optimization by Design of Experiment (DOE)

Based on the outcomes of the exploratory tests, a Central Composite Design (CCD) model was selected where the molar ratio of reactants, and the catalyst loading were considered independent variables while temperature (100 °C), reaction time (45 min), and magnetic stirring (375 rpm) were held constant. In adherence to the CCD model, 9 distinct experiments were conducted, including two replicates at the central point, with the experiments being executed in a randomized order. The values of the studied variables are presented in Table 3. Molecular weight (MW), polydispersity (PD), and yield were determined through Gel Permeation Chromatography (GPC) and Proton Nuclear Magnetic Resonance (^{1}H-NMR) analyses, with results presented in Table 3.

From the experimental outcomes, a Design of Experiment (DOE) model was constructed, taking into consideration the influence of individual factors such as catalyst loading (cat) and stoichiometric ratio (SR), their quadratic effects, and their interactions. Consequently, the following model equations were derived to estimate the dependent variables:

$$\text{Yield \%} = 327.3 - 115.2 \cdot \text{cat} - 486 \cdot \text{SR} + 58.6 \cdot \text{cat}^2 + 254.5 \cdot \text{SR}^2 + 35.9 \cdot \text{cat} \cdot \text{SR} \tag{1}$$

$$\text{PD} = 0.24 - 1.39 \cdot \text{cat} + 2.22 \cdot \text{SR} - 0.510 \cdot \text{cat}^2 - 0.92 \cdot \text{SR}^2 + 2.31 \cdot \text{cat} \cdot \text{SR} \tag{2}$$

$$\text{MW} = 338054 - 134580 \cdot \text{cat} - 684115 \cdot \text{SR} + 38636 \cdot \text{cat}^2 + 359170 \cdot \text{SR}^2 + 95906 \cdot \text{cat} \cdot \text{SR} \tag{3}$$

Subsequently, the calculated values of MW, PD, and yield from the DOE model equations were compared with the experimental values, as shown in Figure 5. Notably, the model exhibited good predictive accuracy for yield and polydispersity, closely approximating the experimental data. However, discrepancies were observed in the predictive accuracy for MW, including negative values. This may be attributed to the dependencies of MW on omitted variables such as mixing speed, efficiency, and density within the DOE model.

The response surface plots (Figure 6) were derived from the DOE calculations to visualize the behavior of the three independent variables as a function of catalyst loading and the stoichiometric ratio of the reactants.

Based on the combined results from the DOE model, we determined the optimal polymerization conditions by defining target values for yield %, polydispersity, and molecular weight (though the latter was used as an approximate guide due to its lower reliability).

The following criteria were established:
- Molecular weight (Mw) > 24000 g mol^{-1};
- Yield $> 80\%$;
- Polydispersity ranging between 2 and 2.3. This interval was chosen as a compromise between achieving a good polymer yield and limiting the parasitic "cross-linking" reactions.

Figure 6 illustrates the graph obtained under the specified conditions. The white area delineates the reaction conditions where all three requirements are fulfilled. Consequently, a test was conducted within this region, employing a catalyst loading of 0.5% and a divinyl/diol stoichiometric ratio of 1.15/1, to validate the DOE model. The experimental results from this test, presented in Table 4, underscore the model's robust predictive capacity, enabling the optimization of the parameters under study.

The polyacetal prepared in the best conditions, at 100 °C with a divinyl ether/diol molar ratio of 1.15/1 and Amberlyst 15

Table 3. Experimental tests conducted for the DOE model: all tests were performed on a 1 g scale of diol.

Entry	Test Order	Catalyst Loading (%)	Molar Ratio (Divinyl/Diol)	Yield %[a]	PDb	MW (g mol^{-1})[b]
1	5	0.32	0.86	76	1.6	2100
2	9	0.32	1.14	87	2.1	33000
3	10	0.88	0.86	71	1.6	1700
4	1	0.88	1.14	87	2.4	48000
5	3	0.20	1.00	84	1.6	1900
6	6	1.00	1.00	73	1.9	3900
7	2	0.60	0.80	71	1.5	1700
8	7	0.60	1.20	88	2.0	15200
9	4	0.60	1.00	73	1.9	3700
10	11	0.60	1.00	66	1.8	3500
11	8	0.60	1.00	70	1.9	4200

[a] Determined by ^{1}H NMR; [b] Determined by GPC.

ChemSusChem

Research Article
doi.org/10.1002/cssc.202402154

Chemistry Europe
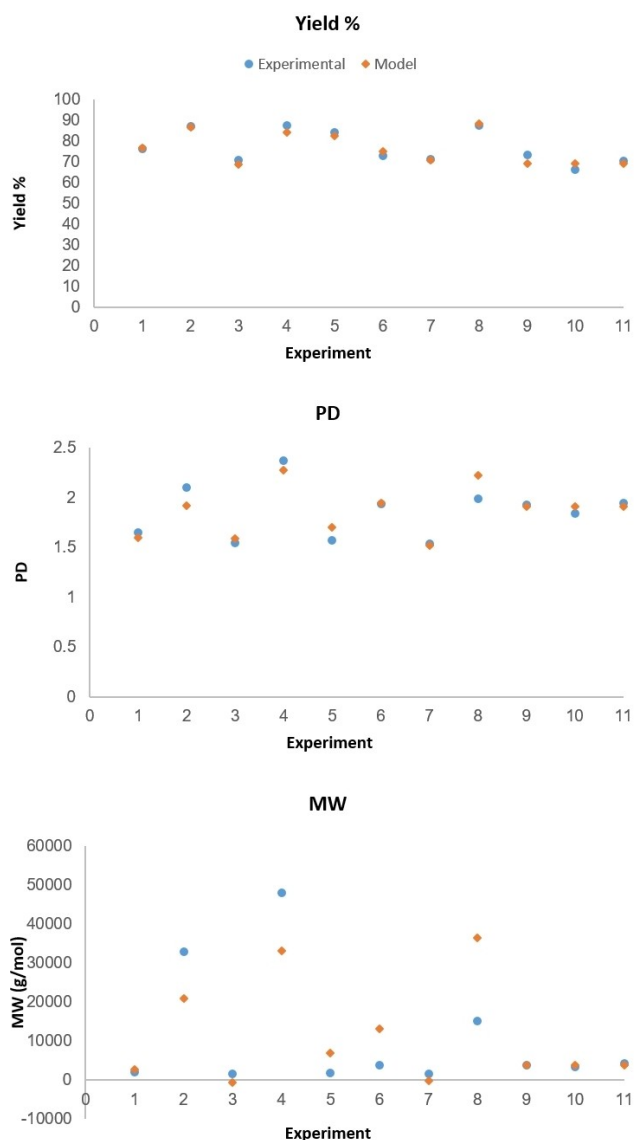European Chemical
Societies Publishing

Figure 5. Experimental and predicted DOE results.

as catalyst (0.5 mol%), was analyzed via DSC and TGA. The second heating scan of DSC showed that the polyacetal presents an amorphous behavior with a T_g of $-73\,°C$ (Figure S5). This value is in agreement with previous studies,[38] and can be ascribed to the flexibility of the aliphatic chain in the repeating unit. TGA analysis in nitrogen (Figure S6) showed that the polyacetal is stable up to $220\,°C$ (T_{onset}). Moreover, after $400\,°C$, no residues were visible, indicating a complete degradation of the polymer. Hashimoto et al. reported the same degradation behavior and observed that polyacetals with different structures all showed high thermal stability.[38] The derivative curve

showed that degradation occurred in different steps, with a maximum degradation rate at $370\,°C$.

Controlled Degradation of the Polyacetal

After fully optimizing the synthesis and determining the material's main thermo-stability domain, the polyacetal architecture was tested to understand if a controlled degradation of the acetal units could be triggered when treated in heterogeneous "real-like" conditions as a heterogeneous material, at room temperature, in water with different pH values. Figure 7 shows the percentage of molecular weight decrement from the initial value of the same batch of polyacetal stirred in water at pH 10, 7, and 4 for 42 days. As observed by the GPC results reported in Table S1, the pH environment impacted differently on the stability of the material resulting in a complete degradation of the molecular weight at pH 4, while at a neutral pH, after an initial 15% degradation the material maintained a stable Mw. Finally, the degradation of the material resulted negligible for pH 10. This preliminary test demonstrated that the polyacetal can be considered a pH-responsive material, being degradable at acidic pH while maintaining a stable structure in terms of molecular weight at basic pH values.

Conclusions

This work addresses the recalcitrant nature of polymeric materials by reinventing and optimizing a macromolecular architecture based on acetal connecting units. The polymerization was performed through a step-growth polyaddition of 1,4-butanediol and 1,4-butanediol divinyl ether, catalyzed by a heterogeneous protic acid (Amberlyst 15) in a solvent-free, scalable process. Mechanistic studies, combining polymerization tests with the synthesis of model compounds, revealed a complex panorama of chemical pathways, including polymeric degradation, cross-linking, and cyclization processes. These pathways are primarily affected by the reagent's stoichiometry and the catalyst loading. The optimal procedure was achieved through a Design of Experiment (DOE) approach, which optimized reagents conversion, polydispersity, and molecular weight. This resulted in a high molecular weight polymer (> 30000 g mol^{-1}), being achieved in just 30 minutes of reaction at $100\,°C$. While presenting thermal properties suitable for industrial processing and compounding (i.e. amorphous character and thermal stability up to $220\,°C$), the resulting material demonstrated a pronounced tendency to hydrolyze only in an acid environment, with complete macromolecular degradation occurring within one month. The reported results represent a

Table 4. Results and model predictions of optimized test condition.

Test condition		Experimental results			Model prediction		
Catalyst Loading (%)	Divinyl/Diol Moles	MW (g mol^{-1})	Yield %	PD	MW (g mol^{-1})	Yield %	PD
0.5	1.15	23800	90	1.91	24400	84	2.08

ChemSusChem

Research Article
doi.org/10.1002/cssc.202402154

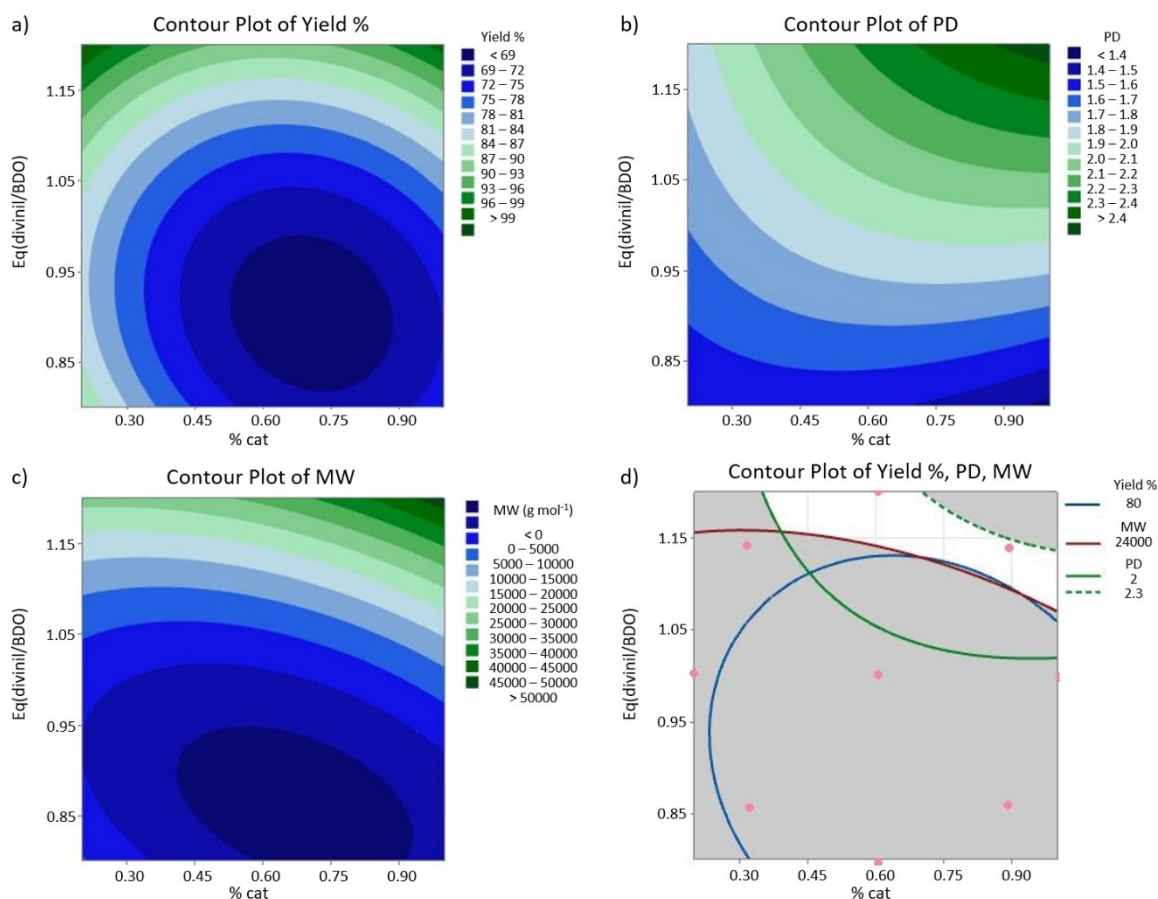**Chemistry Europe**
European Chemical
Societies Publishing

Figure 6. Response surface plots for Yield % (a), PD (b), and MW (c). DOE graph obtained under the specified conditions (d). The blue line delimits % polyacetal higher than 80%, the red line delimits molecular weight over 24000 g mol^{-1}, green lines delimit the area with polydispersity between 2 and 2.3. Pink dots highlight the experiments conducted. The white area delineates the reaction conditions where all three requirements are fulfilled.
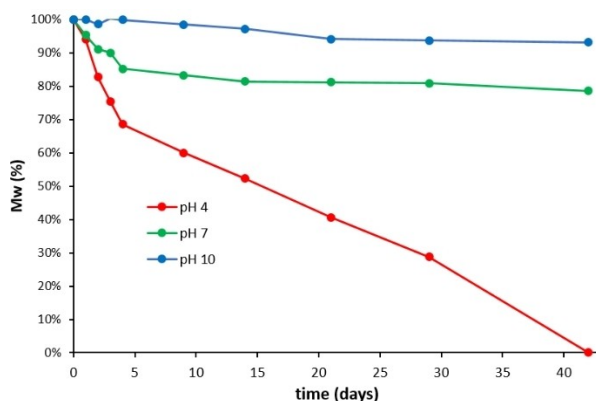

Figure 7. Molecular weight (%) of polyacetal after incubation in aqueous buffer solutions at different pH.

milestone in the design and synthesis optimization of architectures suitable as pH-sensitive components for new-concept adhesives in recyclable multilayer materials or as pH-responsive structural units in novel degradable thermosetting materials.

Conflict of Interests

The authors declare no conflict of interest.

Data Availability Statement

The data that support the findings of this study are available in the supplementary material of this article.

ChemSusChem

Research Article
doi.org/10.1002/cssc.202402154

Chemistry Europe
European Chemical
Societies Publishing

[1] R. Auvergne, S. Caillol, G. David, B. Boutevin, J.-P. Pascault, *Chem. Rev.* **2014**, *114*, 1082–1115.

[2] Y. Liu, Z. Yu, B. Wang, P. Li, J. Zhu, S. Ma, *Green Chem.* **2022**, *24*, 5691–5708.

[3] S. Thiyagarajan, E. Maaskant-Reilink, T. A. Ewing, M. K. Julsing, J. Van Haveren, *RSC Adv.* **2022**, *12*, 947–970.

[4] S. Kakadellis, G. Rosetto, *Science* **2021**, *373*, 49–50.

[5] A. Rahimi, J. M. García, *Nat. Chem. Rev.* **2017**, *1*, 0046.

[6] L. Kárpáti, F. Fogarassy, D. Kovácsik, V. Vargha, *J. Polym. Environ.* **2019**, *27*, 2167–2181.

[7] J. Datta, K. Błażek, M. Włoch, R. Bukowski, *J. Polym. Environ.* **2018**, *26*, 4415–4429.

[8] Y. Deng, Q. Zhang, D. H. Qu, H. Tian, B. L. Feringa, *Angew. Chem.* **2022**, *134*, e202209100.

[9] T. Liu, B. Zhao, J. Zhang, *Polymer* **2020**, *194*, 122392.

[10] N. Jarach, H. Dodiuk, *Biobased Adhesives: Sources, Characteristics and Applications* **2023**, pp. 427–461.

[11] K. R. Mulcahy, A. F. R. Kilpatrick, G. D. J. Harper, A. Walton, A. P. Abbott, *Green Chem.* **2022**, *24*, 36–61.

[12] K. M. A. Kaiser, T. Ginzinger, *Recycling* **2021**, *6*, 47.

[13] X. Kuang, G. Liu, X. Dong, X. Liu, J. Xu, D. Wang, *J. Polym. Sci. Part A* **2015**, *53*, 2094–2103.

[14] Y. Min, S. Huang, Y. Wang, Z. Zhang, B. Du, X. Zhang, Z. Fan, *Macromolecules* **2015**, *48*, 316–322.

[15] M. Delahaye, J. M. Winne, F. E. Du Prez, *J. Am. Chem. Soc.* **2019**, *141*, 15277–15287.

[16] Z. Feng, J. Hu, H. Zuo, N. Ning, L. Zhang, B. Yu, M. Tian, *ACS Appl. Mater. Interfaces* **2018**, *11*, 1469–1479.

[17] H. Memon, H. Liu, M. A. Rashid, L. Chen, Q. Jiang, L. Zhang, Y. Wei, W. Liu, Y. Qiu, *Macromolecules* **2020**, *53*, 621–630.

[18] F. Song, Z. Li, P. Jia, M. Zhang, C. Bo, G. Feng, L. Hu, Y. Zhou, *J. Mater. Chem. A* **2019**, *7*, 13400–13410.

[19] T. Hashimoto, H. Meiji, M. Urushisaki, T. Sakaguchi, K. Kawabe, C. Tsuchida, K. Kondo, *J. Polym. Sci. Part A* **2012**, *50*, 3674–3681.

[20] A. Yamaguchi, T. Hashimoto, Y. Kakichi, M. Urushisaki, T. Sakaguchi, K. Kawabe, K. Kondo, H. Iyo, *J. Polym. Sci. Part A* **2015**, *53*, 1052–1059.

[21] X. Lin, K. Ge, N. He, X. Chen, P. Li, M. Dong, W. Li, *Adv. Synth. Catal.* **2021**, *363*, 4332–4337.

[22] M. L. Jawor, B. M. Ahmed, G. Mezei, *Green Chem.* **2016**, *18*, 6209–6214.

[23] I. Karamé, M. Alame, A. Kanj, G. N. Baydoun, H. Hazimeh, M. el Masri, L. Christ, *C. R. Chim.* **2011**, *14*, 525–529.

[24] B. M. Smith, A. E. Graham, *Tetrahedron Lett.* **2011**, *52*, 6281–6283.

[25] A. R. Trifoi, P. Ş. Agachi, T. Pap, *Renewable Sustainable Energy Rev.* **2016**, *62*, 804–814.

[26] S. Krompiec, M. Penkala, K. Szczubiałka, E. Kowalska, *Coord. Chem. Rev.* **2012**, *256*, 2057–2095.

[27] Y. Chiang, A. J. Kresge, *J. Org. Chem.* **1985**, *50*, 5038–5040.

[28] J. Read, *J. Chem. Soc. Trans.* **1912**, *101*, 2090–2094.

[29] A. Hufendiek, S. Lingier, F. E. Du Prez, *Polym. Chem.* **2019**, *10*, 9–33.

[30] S. Samanta, D. R. Bogdanowicz, H. H. Lu, J. T. Koberstein, *Macromolecules* **2016**, *49*, 1858–1864.

[31] Q. Li, S. Ma, S. Wang, W. Yuan, X. Xu, B. Wang, K. Huang, J. Zhu, *J. Mater. Chem. A* **2019**, *7*, 18039–18049.

[32] Q. Li, S. Ma, S. Wang, Y. Liu, M. A. Taher, B. Wang, K. Huang, X. Xu, Y. Han, J. Zhu, *Macromolecules* **2020**, *53*, 1474–1485.

[33] A. Moreno, M. Morsali, M. H. Sipponen, *ACS Appl. Mater. Interfaces* **2021**, *13*, 57952–57961.

[34] M. J. Heffernan, N. Murthy, *Bioconjugate Chem.* **2005**, *16*, 1340–1342.

[35] S. Penczek, *J. Polym. Sci. Part A* **2000**, *38*, 1919–1933.

[36] R. S. Velichkova, V. B. Gancheva, *J. Polym. Sci. Part A* **1987**, *25*, 2561–2568.

[37] E. Ruckenstein, H. Zhang, *J. Polym. Sci. Part A* **2000**, *38*, 1848–1851.

[38] T. Hashimoto, K. Ishizuka, A. Umehara, T. Kodaira, *J. Polym. Sci. Part A* **2002**, *40*, 4053–4064.

[39] H. Otsuka, T. Endo, *Macromolecules* **1999**, *32*, 9059–9061.

[40] T. Fuoco, *Angew. Chem. Int. Ed.* **2021**, *60*, 15482–15489.

[41] A. Vitale, M. Cominotti, B. Ameduri, R. Bongiovanni, *Eur. Polym. J.* **2016**, *82*, 122–131.

[42] M. D. Fernandez, M. J. Fernandez, P. Hoces, *React. Funct. Polym.* **2008**, *68*, 39–56.

[43] V. V. Pchelintsev, A. Y. Sokolov, G. E. Zaikov, *Polym. Degrad. Stab.* **1988**, *21*, 285–310.

[44] H. Kudo, M. Fukunaga, K. Shiotsuki, H. Takeda, H. Yamamoto, T. Kozawa, T. Watanabe, *React. Funct. Polym.* **2018**, *131*, 361–367.

[45] M. Rostagno, E. J. Price, A. G. Pemba, I. Ghiriviga, K. A. Abboud, S. A. Miller, *J. Appl. Polym. Sci.* **2016**, *133*, 44089.

[46] J. Rickerby, R. Prabhakar, M. Ali, J. Knowles, S. Brocchini, *J. Mater. Chem.* **2005**, *15*, 1849–1856.

[47] A. Moreno, G. Lligadas, J. C. Ronda, M. Galià, V. Cádiz, *Eur. Polym. J.* **2018**, *108*, 348–356.

[48] A. Moreno, G. Lligadas, J. C. Ronda, M. Galià, V. Cádiz, *Polym. Chem.* **2019**, *10*, 5215–5227.

[49] M. Rahaman, N. S. Graca, C. S. M. Pereira, A. E. Rodrigues, *Chem. Eng. J.* **2015**, *264*, 258–267.

[50] S. S. Hwang, C. G. Cho, H. Kim, *Electrochem. Commun.* **2010**, *12*, 916–919.

[51] X. Hong, O. McGiveron, A. K. Kolah, A. Orjuela, L. Peereboom, C. T. Lira, D. J. Miller, *Chem. Eng. J.* **2013**, *222*, 374–381.

[52] E. Cabianca, F. Chéry, P. Rollin, A. Tatibouët, O. De Lucchi, *Tetrahedron Lett.* **2002**, *43*, 585–587.